Structure and high-temperature properties of the (Sr,Ca,Y)(Co, Mn)O$_{3-y}$ perovskites — perspective cathode materials for IT-SOFC

Ph.S. Napolsky [a], O.A. Drozhzhin [a], S.Ya. Istomin [a,*], S.M. Kazakov [a], E.V. Antipov [a], A.V. Galeeva [b], A.A. Gippius [b], G. Svensson [c], A.M. Abakumov [d], G. Van Tendeloo [d]

[a] Department of Chemistry, Moscow State University, Leninskie Gory, Moscow 119991, Russia
[b] Department of Physics, Moscow State University, Leninskie Gory, Moscow 119991, Russia
[c] Department of Materials and Environmental Chemistry, Stockholm University, Stockholm S-10691, Sweden
[d] EMAT, University of Antwerp, Groenenborgerlaan, Antwerp 171, B-2020, Belgium

ABSTRACT

Oxygen deficient perovskites Sr$_{0.75}$Y$_{0.25}$Co$_{1-x}$Mn$_x$O$_{3-y}$, $x=0.5$ and 0.75, were prepared by using the citrate route at 1373–1573 K for 48 h. The cubic Pm-3m perovskite structure for $x=0.5$ was confirmed by electron diffraction study and refined using neutron powder diffraction (NPD) data. For $x=0.75$, the superstructure corresponding to $a=\sqrt{2}\times a_{per}$, $b=2\times a_{per}$, $c=\sqrt{2}\times a_{per}$ ($a^0b^-b^-$ tilt system, space group $Imma$) was revealed by electron diffraction. The solid solution Sr$_{0.75-x}$Ca$_x$Y$_{0.25}$Co$_{0.25}$Mn$_{0.75}$O$_{3-y}$, $0.1\leq x\leq 0.6$ and compound Ca$_{0.75}$Y$_{0.25}$Mn$_{0.85}$Co$_{0.15}$O$_{2.92}$ were prepared in air at 1573 K for 48 h. The crystal structure of Ca$_{0.75}$Y$_{0.25}$Mn$_{0.85}$Co$_{0.15}$O$_{2.92}$ was refined using NPD data (S.G. $Pnma$, $a=5.36595(4)$, $b=7.5091(6)$, $c=5.2992(4)$ Å, $R_p=0.057$, $R_{wp}=0.056$, $\chi^2=4.26$). High-temperature thermal expansion properties of the prepared compounds were studied in air using both dilatometry and high-temperature X-ray powder diffraction data (HTXRPD). They expanding non-linearly at 298–1073 K due to the loss of oxygen at high temperatures. Calculated average thermal expansion coefficients (TECs) for Sr$_{0.75}$Y$_{0.25}$Co$_{1-x}$Mn$_x$O$_{3-y}$, $x=0.5$, 0.75 and Ca$_{0.75}$Y$_{0.25}$Mn$_{0.85}$Co$_{0.15}$O$_{2.92(1)}$ are 15.5, 15.1, and 13.8 ppm K^{-1}, respectively. Anisotropy of the thermal expansion along different unit cell axes was observed for Sr$_{0.15}$Ca$_{0.6}$Y$_{0.25}$Co$_{0.25}$Mn$_{0.75}$O$_{3-y}$ and Ca$_{0.75}$Y$_{0.25}$Mn$_{0.85}$Co$_{0.15}$O$_{2.92}$. Conductivity of Sr$_{0.75}$Y$_{0.25}$Co$_{1-x}$Mn$_x$O$_{3-y}$, $x=0.5$ and 0.75 increases with the temperature reaching 110 S/cm for $x=0.5$ and 44 S/cm for $x=0.75$ at 1173 K. Samples of Sr$_{0.75-x}$Ca$_x$Y$_{0.25}$Co$_{0.25}$Mn$_{0.75}$O$_{3-y}$, $0.1\leq y\leq 0.6$ were found to be n-type conductors at room temperature with the similar temperature dependence of the conductivity and demonstrated the increase of the σ value from ∼1 to ∼50 S/cm as the temperature increases from 300 to 1173 K. Their conductivity is described in terms of the small polaron charge transport with the activation energy (E_p) increasing from 340 to 430 meV with an increase of the calcium content from $x=0$ to $x=0.6$.

© 2012 Elsevier Inc. All rights reserved.

1. Introduction

Oxides with high electronic and oxide-ion conductivity, the so-called mixed ionic-electronic conductors (MIECs), have found wide applications in various high-temperature electrochemical devices such as Solid Oxide Fuel Cells (SOFC) as well as in dense ceramic membranes for separating oxygen from gas mixtures. A-site doped LaMnO$_3$ (e.g., La$_{1-x}$Sr$_x$MnO$_3$ or LSM) is used as a cathode in combination with yttria-stabilized zirconia (YSZ) as electrolyte in SOFC operating at high temperatures 900–1000 °C [1]. The high operating temperatures lead to a limited life-time of the SOFC mainly due to the chemical reactions between different components. Except low chemical activity toward reaction with neighboring components of SOFC, other requirements for SOFC materials include the high conductivity and thermal expansion coefficient (TEC) matching with other components. Therefore a number of efforts have been made to develop SOFC operating at 500–700 °C (so-called intermediate temperature SOFC or IT-SOFC). However, novel materials are needed for these IT-SOFCs to retain the high performance at this temperature range. One possible candidate to substitute LSM as a cathode material in IT-SOFC could be doped LaCoO$_3$. Cobaltites are known to be superior in comparison with LSM both in terms of electronic and oxide-ion conductivity [2]. However, they possess high chemical reactivity towards neighboring SOFC components and high thermal expansion coefficients.

TEC in solids depends on the strength of the interatomic bonds and arrangement of atoms in their crystal structures. Particularly

in perovskites, TEC seems to be dependent on the distortion of the perovskite structure or octahedral tilting. Moreover, the thermal expansion behavior of solids can be changed with temperature. Main reasons for that are variations of the chemical composition with temperature (the so-called chemical expansion), structural and magnetic transitions. Cobaltites containing Co^{3+} cations are rare examples of the system where the thermal expansion changes with temperature due to transitions between low (LS, $t_2{}_g^6 e_g^0$) and high (HS, $t_2{}_g^4 e_g^2$) spin states of Co^{3+} [3]. This happens because of a substantial difference in ionic radii of LS and HS Co^{3+} (rCo^{3+} (LS)=0.545 Å; rCo^{3+} (HS)=0.61 Å [4]). An example of the influence of the LS/HS spin transition on TEC in cobaltites can be seen when comparing high temperature (298–1273 K) TEC values of $LaMO_3$, M – a 3d-metal, where the maximum TEC of 21 ppm K^{-1} [5] is observed for $LaCoO_3$ in comparison with 10.7 ppm K^{-1} for $LaMnO_3$ [6], 9.5 ppm K^{-1} for $LaFeO_3$ [7] and 13.5 ppm K^{-1} for $LaNiO_3$ [7]. One way to decrease TEC of cobaltites is the partial substitution of Co^{3+} by other transition metal cations like Mn or Fe [8–13].

Recently oxygen-deficient cobaltites $Sr_{0.7}Y_{0.3}CoO_{3-y}$ and $Sr_{0.7}Ho_{0.3}CoO_{3-y}$ with the layered perovskite-related structure (so-called 314-phases [14,15]) were found to demonstrate good performance as cathode materials in IT-SOFC [16,17]. Some years ago we have reported on the study of the high-temperature thermal expansion and conductivity properties of cobaltite $Sr_{0.75}Y_{0.25}CoO_{2.625}$ with the same crystal structure and its Fe-doped derivatives $Sr_{0.75}Y_{0.25}Co_{1-x}Fe_xO_{2.625+y}$ [18]. It was found that a partial substitution of cobalt by iron leads to a decrease in TEC, but only at moderate ($T < 673$ K) temperature. In these compounds the presence of iron results in an increase of the oxygen content in comparison with the un-doped 314-phase due to the higher stability of Fe^{4+} in comparison with Co^{4+}. This in turn leads to an increased contribution of the chemical expansion on TEC due to the formation of oxygen vacancies at high temperature. We have therefore replaced Fe with Mn and recently reported on good performance of mixed perovskites $Sr_{0.75}Y_{0.25}Co_{0.5}Mn_{0.5}O_{3-y}$ [19] and $Ca_{0.75}Y_{0.25}Co_{0.15}Mn_{0.85}O_{3-y}$ [20] as cathodes in electrolyte-supported SOFCs.

In the present paper we report on the synthesis, crystal structure, high-temperature thermal expansion and conductivity properties of Mn-substituted 314-phase $Sr_{0.75}Y_{0.25}Co_{1-x}Mn_xO_{3-y}$, x=0.5, 0.75. Bearing in mind probable variation of TEC for perovskite-related oxides by changing their crystal structure symmetry, we have performed the substitution of large Sr^{2+} cation in $Sr_{0.75}Y_{0.25}Co_{0.25}Mn_{0.75}O_{3-y}$ by smaller Ca^{2+} ($r(Ca^{2+})$= 1.35 Å); $r(Sr^{2+})$=1.44 Å [4]) in order to increase the distortion of the perovskite structure by decreasing the so-called tolerance factor (t-factor [21]). The crystal structure, thermal expansion and high-temperature transport properties of the prepared $Sr_{0.75-y}Ca_yY_{0.25}Co_{0.25}Mn_{0.75}O_{3-y}$, $0.1 \leq y \leq 0.6$ compounds were also studied in this work.

2. Experimental

Samples of $Sr_{0.75}Y_{0.25}Co_{1-x}Mn_xO_{3-y}$, x=0.25, 0.5 and 0.75, were prepared using the citrate route. Stoichiometric amounts of $SrCO_3$, Y_2O_3, $Mn(CH_3COO)_2 \times 3.69H_2O$ and $Co(NO_3)_3 \times 6H_2O$ (all 99% or higher) were dissolved in a melt of citric acid. The mixture was slowly heated in air to 1173 K and fired for 12 h, followed by re-grinding, pressing into pellets and sintering in air at 1373–1573 K for 48 h.

Samples of $Sr_{0.75-x}Ca_xY_{0.25}Co_{0.25}Mn_{0.75}O_{3-y}$, $0.0 < x \leq 0.75$, step Δx=0.1, were prepared by annealing stoichiometric mixtures of $SrCO_3$, $CaCO_3$, Y_2O_3, MnO_2 and Co_3O_4 at 1573 K for 48 h with one intermediate regrinding at 1173 K for 24 h. The

oxygen content of the samples was determined by the iodometric titration [22].

Phase purity of the compounds was checked by X-ray powder diffraction (XRPD) recorded with a Huber G670 Guinier camera ($CuK_{\alpha1}$ radiation, image foil detector, Ge monochromator). High-temperature X-ray powder diffraction data (HTXRPD) were collected using Bruker D8-Advance diffractometer ($CuK_{\alpha1}$ radiation, Vantec PSD) equipped with a high-temperature camera XRK-900 (Anton Paar). Unit cell parameters at different temperatures were refined by the full profile refinement program Topas-3 taking into account the samples displacement from the goniometer center, due to sample and holder thermal expansions.

Neutron powder diffraction (NPD) data for $Sr_{0.75}Y_{0.25}Co_{0.5}Mn_{0.5}O_{2.73}$ and $Ca_{0.75}Y_{0.25}Co_{0.15}Mn_{0.85}O_{2.92}$ were collected in ISIS on Polaris and GEM TOF diffractometers, respectively. Refinements of the crystal structures were performed using the GSAS program package [23].

For the electron diffraction (ED) and high-resolution electron microscopy (HREM) studies, a small amount of a sample was grinded in an agate mortar under ethyl alcohol. The resulting suspension was deposited onto a carbon film supported by a copper grid. ED patterns were recorded at a Philips CM-20 (acceleration voltage of 200 kV) transmission electron microscope. High-resolution electron microscopy (HREM) study was performed on a JEOL JEM-4000EX transmission electron microscope with an acceleration voltage of 400 kV.

Measurements of the high-temperature transport properties of $Sr_{0.75}Y_{0.25}Co_{1-x}Mn_xO_{3-y}$, x=0.5, 0.75, $Ca_{0.75}Y_{0.25}Co_{0.15}Mn_{0.85}O_{2.92}$ and $Sr_{0.75-y}Ca_yY_{0.25}Co_{0.25}Mn_{0.75}O_{3-\delta}$, $0.1 \leq y \leq 0.6$ were performed in air by 4-probe method in the temperature range of 300–1200 K.

Netzsch 402 C dilatometer operated in air (298–1173, 10 K/min) was used for the thermal expansion coefficient measurements. For this purpose oxide powders were pressed into pellets of 8 mm in diameter and 5–5.5 mm in height and annealed at 1473 K.

3. Results

3.1. Crystal structures of $Sr_{0.75}Y_{0.25}Co_{1-x}Mn_xO_{3-y}$, x=0.25, 0.5 and 0.75

All the prepared cobalt- and manganese-contained samples were black. After synthesis the XRPD patterns of $Sr_{0.75}Y_{0.25}Co_{1-x}Mn_xO_{3-y}$ x=0.5 and 0.75 samples were indexed with cubic (a=3.8205(3) Å) and tetragonal (a=3.8041(3), c=3.8172(7) Å) unit cells, respectively. Weak reflections ($< 1\%$) from CoO were observed in both XRPD patterns, however, no additional reflections indicating a superstructure were present. The sample with x=0.25 was multiphase and contained a cubic perovskite phase with a unit cell parameter a=3.8175(4) Å together with admixtures of Y_2O_3 ($< 10\%$) and SrY_2O_4 ($< 5\%$).

The cubic symmetry and the absence of superstructure reflections were confirmed for $Sr_{0.75}Y_{0.25}Co_{0.5}Mn_{0.5}O_{3-y}$ by the ED study (Fig. 1). Weak superstructure reflections were observed on the ED patterns of the x=0.75 sample (Fig. 2), which required the body-centered aHb $\approx \sqrt{2} \times a_{per}$, $c = \sqrt{2} \times a_{per}$ supercell to be indexed. From the group-theory analysis of tilting distortions in perovskites [24], two possibilities can be suggested which match I-centered unit cell: the $a^0a^0c^-$ tilt system (I 4/mcm space group) and $a^0b^-b^-$ tilt system ($Imma$ space group, $a=\sqrt{2} \times a_{per}$, $b=2 \times a_{per}$, $c=\sqrt{2} \times a_{per}$). Presence of superstructure reflections in the {1 1 0}$_p$ ED pattern ([1 0 0] ED pattern in Fig. 2) does not match the reflection conditions of the I 4/mcm space group, leaving $Imma$ as the only possibility. It should be noted that very weak $hk0$, h-odd, spots are present on the [0 0 1] ED pattern
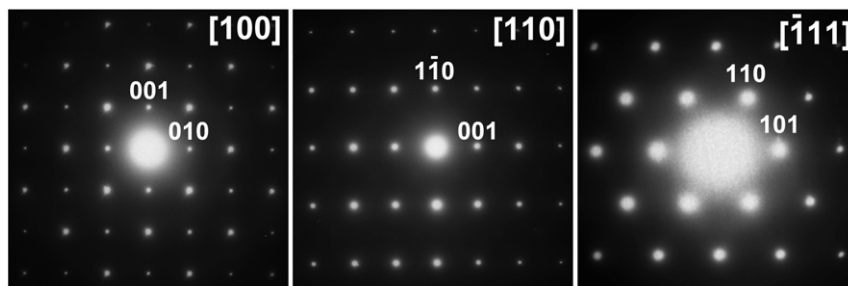
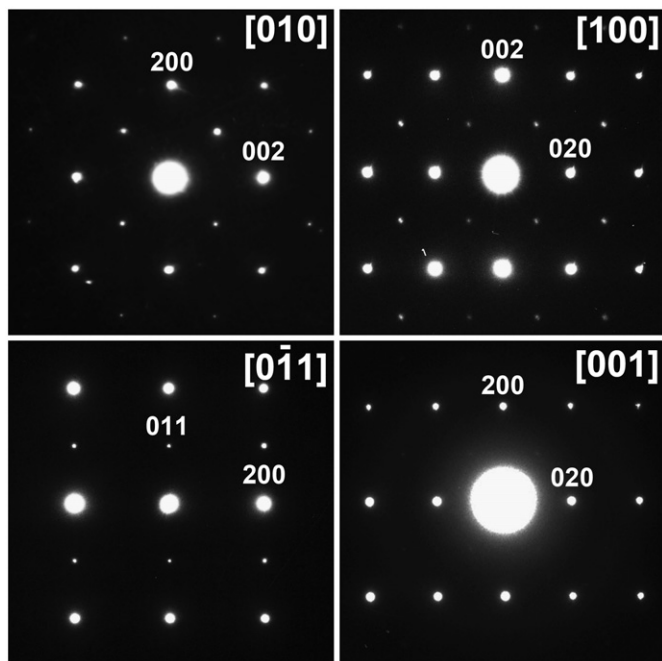**Fig. 1.** SAED patterns of $Sr_{0.75}Y_{0.25}Co_{0.5}Mn_{0.5}O_{3-y}$ with a cubic perovskite structure viewed along [1 0 0] [1 1 0] and [$\bar{1}$ 1 1].

Fig. 2. SAED patterns of $Sr_{0.75}Y_{0.25}Co_{0.25}Mn_{0.75}O_{3-y}$ with an orthorhombically distorted structure ($a=\sqrt{2} \times a_{per}$, $b=2 \times a_{per}$, $c=\sqrt{2} \times a_{per}$, space group *Imma*) viewed along [1 0 0], [0 1 0], [0 $\bar{1}$ 1], [0 0 1].

apparently violating the reflection condition imposed by the *a*-glide plane of the *Imma* space group. However, the appearance of these reflections can be explained by the [1 0 0]/[0 0 1] twinning due to the pseudo-tetragonal structure.

The crystal structure of the cubic perovskite $Sr_{0.75}Y_{0.25}Co_{0.5}Mn_{0.5}O_{y-3}$ was refined using the TOF NPD data. Neither superstructure, nor splitting of the perovskite subcell reflections were observed in the NPD pattern of $Sr_{0.75}Y_{0.25}Co_{0.5}Mn_{0.5}O_{y-3}$. However, some weak reflections ($I < 1\%$) marked with asterisks on Fig. 3, which we could not assigned to known phases, are present on NPD pattern. The crystal data, atomic coordinates, occupancies and displacement parameters are given in Table 1. I_{obs}, I_{calc} and $I_{obs-cal}$ neutron diffraction profiles are shown in Fig. 3. Due to the similar scattering lengths for Sr and Y (0.702 and 0.775 10^{-12} cm, respectively) it was not possible to refine the Sr/Y ratio. Therefore the Sr/Y ratio was fixed to the nominal value of Sr/Y=0.75:0.25. Refinement of the Co/Mn ratio (scattering lengths for Co and Mn are 0.249 and -0.373 10^{-12} cm, respectively) resulted in a value close to the nominal composition, Table 1. The oxygen content of the phase calculated from the refinement of the occupancy of the oxygen position corresponds to the formula $Sr_{0.75}Y_{0.25}Co_{0.5}Mn_{0.5}O_{2.73(1)}$ and is in good agreement with that of determined by the iodometric titration.

3.2. Crystal structure of $Sr_{0.75-x}Ca_xY_{0.25}Co_{0.25}Mn_{0.75}O_{3-y}$, $0.0 < x \leq 0.75$ and $Ca_{0.75}Y_{0.25}Co_{0.15}Mn_{0.85}O_{3-y}$.

Single-phase samples of $Sr_{0.75-x}Ca_xY_{0.25}Co_{0.25}Mn_{0.75}O_{3-y}$ were prepared for the compositional range $0.1 \leq x \leq 0.6$. No splitting of the perovskite subcell reflections was observed in the XRPD patterns of the $0.1 \leq x \leq 0.3$ samples. However, the presence of a weak additional reflection with $d < 2.29$ Å, which can be indexed as (3 1 1) in a doubled perovskite unit cell with $a=2 \times a_{per}$ or as (2 1 1), (0 1 3) or (1 1 2) in an orthorhombic unit cell with $a=\sqrt{2} \times a_{per}$, $b=2 \times a_{per}$, $c=\sqrt{2} \times a_{per}$, was observed in the XRPD patterns. The intensity of this reflection increases with the calcium content. Taking into account that undoped $Sr_{0.75}Y_{0.25}Co_{0.25}Mn_{0.75}O_{3-y}$ crystallizes in an orthorhombic perovskite-based unit cell (*Imma*, $a=\sqrt{2} \times a_{per}$, $b=2 \times a_{per}$, $c=\sqrt{2} \times a_{per}$), the assumption that the samples with $0.1 \leq x \leq 0.3$ have the same type of crystal structure seems to be reasonable.

In XRPD patterns of the samples $0.4 \leq x \leq 0.6$, in addition to the $d \sim 2.29$ Å reflection, numerous additional reflections were present, which could be indexed with the $a=\sqrt{2} \times a_{per}$, $b=2 \times a_{per}$, $c=\sqrt{2} \times a_{per}$ orthorhombic unit cell (Fig. 4). Reflection conditions, e.g., the presence of reflections with $h+k+l \neq 2n$ in XRPD patterns of the $0.4 \leq x \leq 0.6$ samples (see inset in Fig. 4), show that the symmetry of these samples is different in compared to the $x=0.0$ sample and corresponds to the orthorhombic $GdFeO_3$-type structure. The samples with $x \geq 0.7$ were multiphase and contained together with the orthorhombic perovskite phase an admixture of $Ca_2(Mn,Co)O_4$. Unit cell parameters for $Sr_{0.75-x}Ca_xCo_{0.25}Mn_{0.75}O_{3-y}$, $0.1 \leq x \leq 0.75$ determined from the XRPD data are given in Table 2.

ED studies confirm the $GdFeO_3$-type orthorhombic structure of $Sr_{0.05}Ca_{0.7}Co_{0.25}Mn_{0.75}O_{3-y}$. Due to the close *a*- and *c*-unit cell parameters (Table 2), severe twinning is observed in the crystallites (Fig. 5). This is illustrated in Fig. 5a where an electron diffraction pattern is given for the perovskite phase presented in the $Sr_{0.05}Ca_{0.70}Y_{0.25}Co_{0.25}Mn_{0.75}O_{3-y}$ sample. It can be interpreted as a superposition of several diffraction patterns from the orthorhombic $GdFeO_3$-type viewed along [1 0 1] and [0 1 0] (Fig. 5(b) and (c)).

The compositional dependences of the *a*- and *c*-parameters (Fig. 6) show that the orthorhombic distortion of the crystal structure of $Sr_{0.75-x}Ca_xY_{0.25}Co_{0.25}Mn_{0.75}O_{3-y}$ increases with increasing the calcium content (*x*). This happens due to the smaller size of the calcium cation resulting in a decrease of the *t*-factor from 0.973 for $Sr_{0.75}Y_{0.25}Co_{0.25}Mn_{0.75}O_3$ to 0.962 for hypothetical $Ca_{0.75}Y_{0.25}Co_{0.25}Mn_{0.75}O_3$. The largest orthorhombic splitting is observed for the perovskite-related phase in the multiphase $x=0.75$ sample. Its unit cell parameters and volume are clearly out of the general dependence observed for other compositions (Fig. 6). The EDX analysis revealed that this orthorhombic perovskite phase contains less amount of cobalt and its composition corresponds to the formula $Ca_{0.75}Y_{0.25}Co_{0.15}Mn_{0.85}O_{3-y}$. A single-phase sample with this nominal composition was prepared by

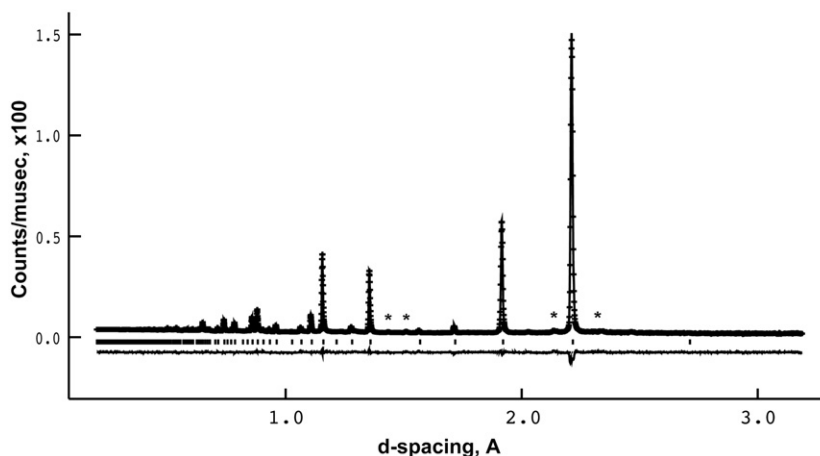**Fig. 3.** Observed, calculated and difference NPD profiles along with peak positions for $Sr_{0.75}Y_{0.25}Co_{0.5}Mn_{0.5}O_{3-y}$. Reflections marked with asterisks belong to unknown admixture phases.

Table 1
Coordinates, occupancies and atomic displacement parameters (ADP) for $Sr_{0.75}Y_{0.25}Co_{0.5}Mn_{0.5}O_{2.73}$ refined from the NPD data (S.G. $Pm3m$, $a=3.82821(2)$ Å; $\chi^2=9.16$, $R_p=0.0459$; $R_{wp}=0.0347$).

Atom, position	X	y	z	ADP U (Å^2) ($\times 100$)	Occupancy
Sr/Y, 1b	½	½	½	0.6(2)	0.75/0.25
Co/Mn, 1a	0	0	0	0.23(8)	0.43(1)/0.57(1)
O, 3d	½	0	0	2.2(2)	0.91(1)
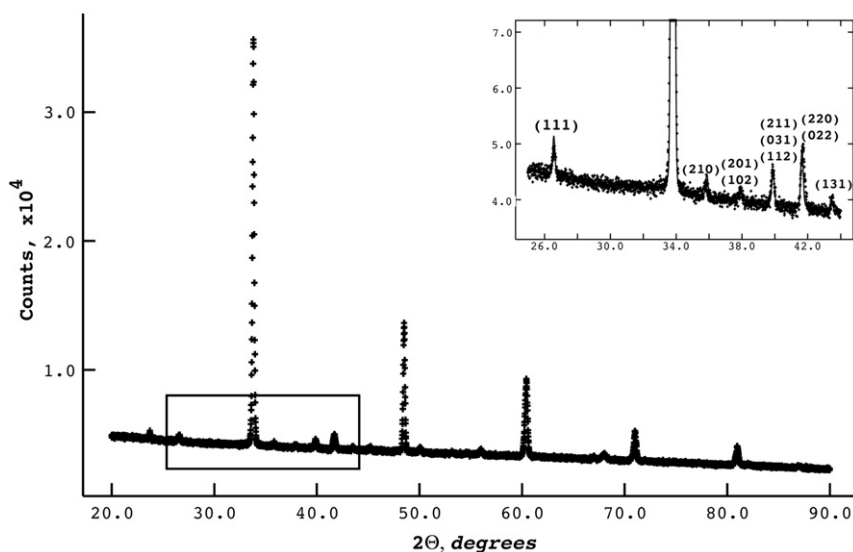
Fig. 4. XRPD pattern for $Sr_{0.15}Ca_{0.6}Y_{0.25}Co_{0.25}Mn_{0.75}O_{3-y}$. Superstructure reflections indicating the formation of the orthorhombic unit cell ($a=\sqrt{2} \times a_{per}$, $b=2 \times a_{per}$, $c=\sqrt{2} \times a_{per}$, S.G. $Pnma$) are shown in the inset. Indexes of the reflections are given in the orthorhombic supercell.

annealing a stoichiometric mixture of $CaCO_3$, Y_2O_3, MnO_2 and Co_3O_4 at 1573 K, 48 h. The oxygen content of the sample determined by the iodometric titration corresponds to $Ca_{0.75}Y_{0.25}Mn_{0.85}Co_{0.15}O_{2.92(1)}$. Surprisingly, this phase has no significant homogeneity range since all attempts to prepare single-phase samples with slightly different Co/Mn or Ca/Y ratios according to formula $Ca_{0.75+z}Y_{0.25-z}Co_{0.15+t}Mn_{0.85-t}O_{3-y}$ were unsuccessful.

The crystal structure of $Ca_{0.75}Y_{0.25}Co_{0.15}Mn_{0.85}O_{2.92}$ was refined using neutron powder diffraction data. There were additional weak ($I<3\%$) reflections from unknown phases present in the NPD pattern (Fig. 7), which could not be accounted for in the Rietveld refinement. Initial atomic coordinates were taken from

the crystal structure of $CaMnO_3$ [25]. The Ca/Y ratio was fixed in accordance with the nominal cation stoichiometry and was thus not refined, while the Co/Mn ratio was refined. The oxygen content of the phase was fixed in accordance with the results of the chemical analysis. Three different models of the distribution of oxygen vacancies were tested. Two models having oxygen vacancies at the 4c or 8d sites of the S.G. $Pnma$ and one with a disordered distribution of oxygen vacancies between these two positions, were tested. No large differences between the results of the refinements in these three structure models were observed. Therefore, the final refinement was performed with a model with a disordered distribution of the oxygen vacancies. The final

atomic coordinates, displacement parameters and selected interatomic distances are given in Table 3. I_{obs}, I_{calc} and $I_{obs-cal}$ diffraction profiles of the NPD curves are shown in Fig. 7.

3.3. High-temperature thermal expansion properties.

3.3.1. $Sr_{0.75}Y_{0.25}Co_{1-x}Mn_xO_{3-y}$, x=0.5 and 0.75.

The samples of $Sr_{0.75}Y_{0.25}Co_{1-x}Mn_xO_{3-y}$, x=0.5 and 0.75, expand non-linearly at 298–1073 K. The increase of TEC with the temperature is accelerated at $T > 600$ K as illustrated in Fig. 8 where the thermal expansion curve for x=0.75 is given together with its first derivative (TEC). The thermogravimetric analysis for x=0.75 clearly shows that the weight of the sample starts to decrease at $T > 600$ K, most probably due to the oxygen loss. Average TECs calculated for the whole temperature range of 298–1073 K are 15.5 and 15.1 ppm K^{-1} for the x=0.5 and 0.75 samples, respectively.

The crystal structure of $Sr_{0.75}Y_{0.25}Co_{0.25}Mn_{0.75}O_{3-y}$ was studied using the high-temperature XRPD data between 298–1073 K. The splitting of the perovskite subcell reflections decreases gradually with increasing the temperature up to 673 K, wherafter the absence of a split indicates a transformation to a cubic perovskite structure. The temperature dependence of the $\sqrt[3]{V}$ (perovskite subcell) for $Sr_{0.75}Y_{0.25}Co_{0.25}Mn_{0.75}O_{3-y}$ is

Fig. 6. Compositional (x) dependence of the unit cell parameters of $Sr_{0.75-x}$ $Ca_xY_{0.25}Co_{0.25}Mn_{0.75}O_{3-y}$, $0.1 \leq x \leq 0.75$. The volume ($V^{1/3}$) dependence is given in the inset. Note that the values corresponding to 0.75 are out of the linear dependence.

Table 2
Unit cell parameters, phase analysis and TEC data for $Sr_{0.75-x}Ca_xY_{0.25}Co_{0.25}$ $Mn_{0.75}O_{3-y}$, $0.0 < x \leq 0.75$.

x	Unit cell parameters (Å)	TEC (ppm K^{-1})[b]
0.1	a=7.6018(7)[a]	16.7
0.2	a=7.5860(6)[a]	16.0
0.3	a=7.5708(5)[a]	15.8
0.4	a=5.3436(1); b=7.5567(2); c=5.3384(1)	15.7
0.5	a=5.3329(2); b=7.5384(3); c=5.3234(2)	15.3
0.6	a=5.3249(1); b=7.5161(2); c=5.3048(1)	15.0
0.7	a=5.3149(2); b=7.4932(3); c=5.2954(2) + Ca$_2$(Mn, Co)O$_4$ (~3%)	–
0.75	a=5.339(2); b=7.487(3); c=5.281(2) +Ca$_2$(Mn,Co)O$_4$ 10%	–

[a] Most probably, an orthorhombic unit cell.
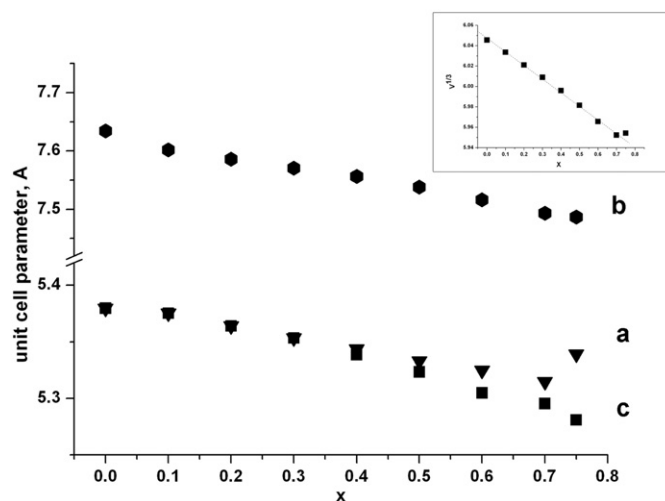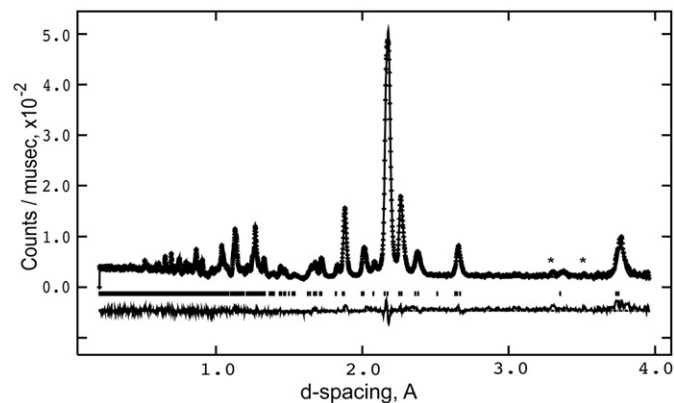[b] TEC is calculated as a difference between relative thermal expansion values at 423 and 1073 K.

Fig. 7. Observed, calculated and difference between them NPD profiles along with peak positions for $Ca_{0.75}Y_{0.25}Co_{0.15}Mn_{0.85}O_{3-y}$. Reflections marked with asterisks belong to unknown admixture phases.

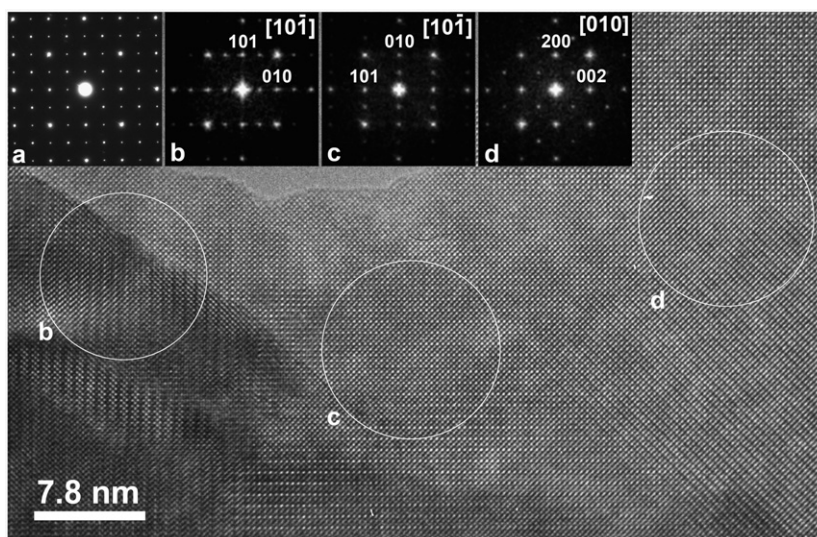**Fig. 5.** HREM image with the corresponding SAED pattern (a) of the perovskite phase in $Sr_{0.05}Ca_{0.7}Y_{0.25}Co_{0.25}Mn_{0.75}O_{3-y}$ sample. FFTs calculated from the marked areas of the crystallite are shown in (b), (c) and (d). Indexes are given for the orthorhombic GdFeO$_3$-type unit cell ($a=\sqrt{2} \times a_{per}$, $b=2 \times a_{per}$, $c=\sqrt{2} \times a_{per}$).

Table 3

Atomic coordinates, displacement parameters (ADP) (Å) and selected interatomic distances (Å) (B) in the crystal structure of $Ca_{0.75}Y_{0.25}Mn_{0.85}Co_{0.15}O_{2.92}$ refined from the NPD data (S.G. *Pnma*, $a=5.36595(4)$, $b=7.5091(6)$, $c=5.2992(4)$ Å, $R_p=0.0570$, $R_{wp}=0.0563$, $\chi^2=4.255$).

(A)

Atom, position	X	y	z	ADP U (Å^2) ($\times 100$)	Occupancy
Ca/Y, 4c	0.0423(4)	0.25	−0.0124(7)	0.83(4)	0.75/0.25
Co/Mn, 4a	0	0	0.5	0.05(6)	0.141(3)/0.859(3)
O1, 4c	0.4834(4)	0.25	0.0728(6)	0.49(5)	0.973
O2, 8d	0.2932(3)	0.0388(3)	−0.2922(3)	0.59(3)	0.973

(B)

Ca/Y–O1=2.352(5), 2.406(3), 2.986(5); Ca/Y–O2=2.320(3) ($\times 2$), 2.553(3) ($\times 2$), 2.615(3) ($\times 2$)
Co/Mn–O1=1.9185(6) ($\times 2$); Co/Mn–O2=1.942(2) ($\times 2$), 1.927(2) ($\times 2$)

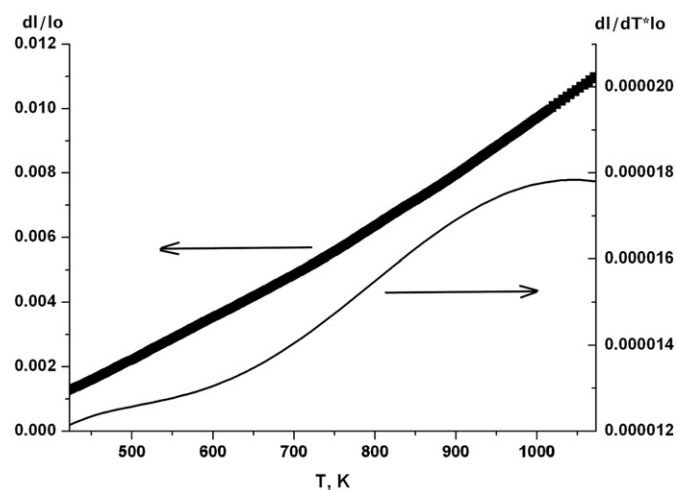**Fig. 8.** Thermal expansion curve (left) together with its first derivative (TEC) (right) for $Sr_{0.75}Y_{0.25}Co_{0.25}Mn_{0.75}O_{3-y}$.

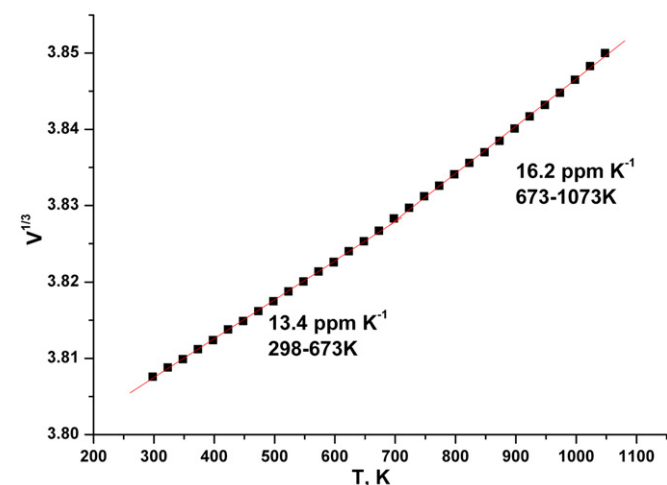**Fig. 9.** Temperature dependence of the $\sqrt[3]{V}$ (perovskite subcell) for $Sr_{0.75}Y_{0.25}Co_{0.25}Mn_{0.75}O_{3-y}$. Note the presence of two different temperature ranges.

shown in Fig. 9. There are two distinct temperature ranges; (i) at 298–673 K the calculated TEC is 13.4 ppm K^{-1}, while (ii) for $T > 673$ K it increases up to 16.2 ppm K^{-1}. Therefore one can conclude that $Sr_{0.75}Y_{0.25}Co_{0.25}Mn_{0.75}O_{3-y}$ at $T > 673$ K undergoes a phase transition from the orthorhombic to cubic perovskite structure.

3.3.2. $Sr_{0.75-x}Ca_xY_{0.25}Co_{0.25}Mn_{0.75}O_{3-y}$, $0.1 \leq x \leq 0.6$ and $Ca_{0.75}Y_{0.25}Mn_{0.85}Co_{0.15}O_{2.92}$

The thermal expansion curves for $Sr_{0.75-x}Ca_xY_{0.25}Co_{0.25}Mn_{0.75}O_{3-y}$, $0.1 \leq x \leq 0.6$ show a non-linear dependence for all studied compositions due to the decrease of the oxygen content at $T > 700$ K, similar to that observed for the $Sr_{0.75}Y_{0.25}Co_{0.25}Mn_{0.75}O_{3-y}$ sample mentioned above. The values of TEC calculated as a difference between relative expansion values at 423 and 1073 K for different calcium content are given in Table 2. There is a slight tendency to the decrease of TEC with increasing of calcium content.

The crystal structures of $Sr_{0.15}Ca_{0.6}Y_{0.25}Co_{0.25}Mn_{0.75}O_{3-y}$ and $Ca_{0.75}Y_{0.25}Mn_{0.85}Co_{0.15}O_{2.92}$ were studied using the HTXRPD data recorded at selected temperatures from 298 to 1073 K. None of the compounds show a phase transition from the GdFeO$_3$-type structure to higher symmetry perovskites up to 1073 K. The temperature dependences of the unit cell parameters for $Sr_{0.15}Ca_{0.6}Y_{0.25}Co_{0.25}Mn_{0.75}O_{3-y}$ and $Ca_{0.75}Y_{0.25}Mn_{0.85}Co_{0.15}O_{2.92}$ are shown on Fig. 10(a) and (b). The orthorhombic splitting of the unit cell parameters decreases with the temperature for both compounds. An anisotropy of the TEC for individual unit cell parameters is observed both for $Sr_{0.15}Ca_{0.6}Y_{0.25}Co_{0.25}Mn_{0.75}O_{3-y}$ and $Ca_{0.75}Y_{0.25}Mn_{0.85}Co_{0.15}O_{2.92}$. The thermal expansion along the *a*-axis is lower in comparison with the expansions along the *b*- and *c*-axes. Thus for $Sr_{0.15}Ca_{0.6}Y_{0.25}Co_{0.25}Mn_{0.75}O_{3-y}$, TEC values of the individual unit cell parameters are TEC(a)=12.4 ppm K^{-1}, TEC(b)=16.7 ppm K^{-1} and TEC(c)=16.8 ppm K^{-1}, whereas for $Ca_{0.75}Y_{0.25}Mn_{0.85}Co_{0.15}O_{2.92}$, TEC(a)=7.1 ppm K^{-1}, TEC(b)=15.3 ppm K^{-1} and TEC(c)=15.9 ppm K^{-1} (298–1073 K). Smaller TEC values of individual unit cell parameters (especially for the *a*-parameter) for $Ca_{0.75}Y_{0.25}Mn_{0.85}Co_{0.15}O_{2.92}$ lead to its lower linear TEC calculated from the temperature dependence of the unit cell volume ($V^{1/3}$): 13.8 ppm K^{-1} in comparison with 15.4 ppm K^{-1} for $Sr_{0.15}Ca_{0.6}Y_{0.25}Co_{0.25}Mn_{0.75}O_{3-y}$.

3.4. High-temperature conductivity properties

3.4.1. $Sr_{0.75}Y_{0.25}CO_{3-y}Mn_xO_{3-y}$, $x=0.5$ and 0.75

The temperature dependence of the conductivity presented as $\log(\sigma \cdot T) - 1/T$ for $Sr_{0.75}Y_{0.25}CO_{3-y}Mn_xO_{3-y}$, $x=0.5$ and 0.75, ceramic samples together with the conductivity data for $Sr_{0.75}Y_{0.25}CoO_{2.625}$ taken from Ref. [18] are given in Fig. 11. For both $x=0.5$ and 0.75 samples the conductivity is substantially lower in comparison with undoped $Sr_{0.75}Y_{0.25}CoO_{2.625}$. Moreover, at high temperature (1173 K) there is a clear tendency for the conductivity to decrease with the manganese content, from 199.1 S/cm for $Sr_{0.75}Y_{0.25}CoO_{2.625}$ [18] to 110 S/cm for $x=0.5$ and 44 S/cm for $x=0.75$.

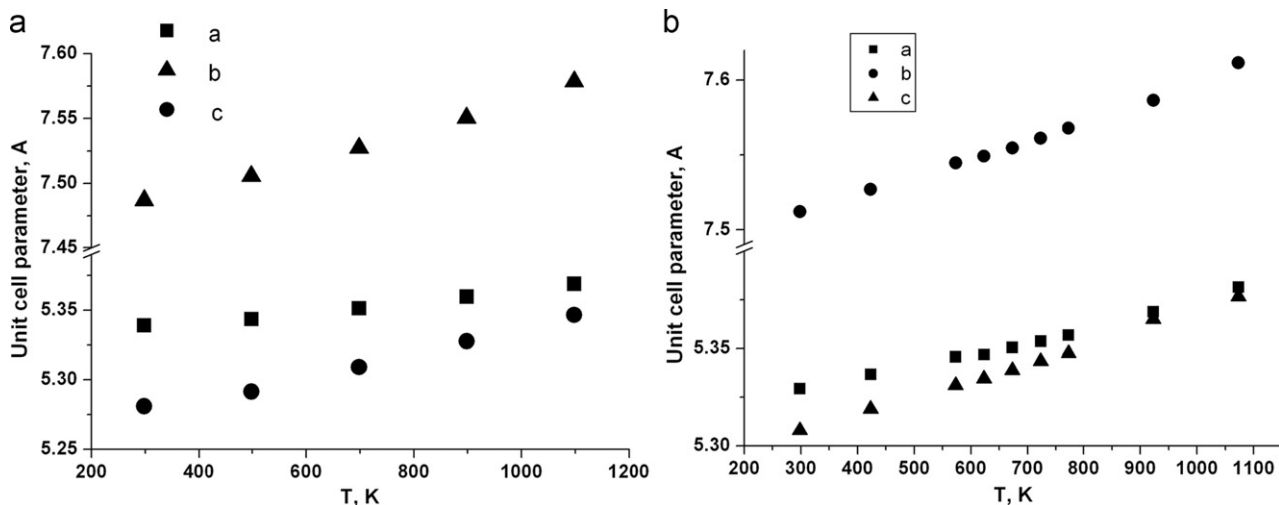**Fig. 10.** Temperature dependence of the unit cell parameters for $Sr_{0.15}Ca_{0.6}Y_{0.25}Co_{0.25}Mn_{0.75}O_{3-y}$ (a) and $Ca_{0.75}Y_{0.25}Mn_{0.85}Co_{0.15}O_{2.92}$ (b).
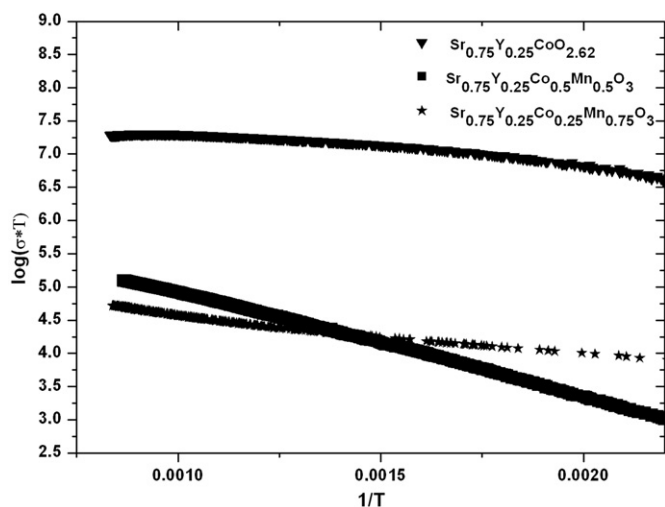

Fig. 11. Temperature dependence of the conductivity presented as $\log(\sigma \cdot T) - 1/T$ for $Sr_{0.75}Y_{0.25}Co_{1-x}Mn_xO_{3-y}$, $x=0.5$ and 0.75, ceramic samples together with the conductivity data for $Sr_{0.75}Y_{0.25}CoO_{2.625}$ from Ref. [18].

Fig. 12. Temperature dependencies of the conductivities for $Sr_{0.75-x}Ca_xY_{0.25}Co_{0.25}Mn_{0.75}O_{3-y}$ in the coordinates $\log(\sigma \cdot T) - 1/T$. The compositional dependence of the calculated E_p is given in the inset.

3.4.2. $Sr_{0.75-x}Ca_xY_{0.25}Co_{0.25}Mn_{0.75}O_{3-y}$, $0.1 \leq x \leq 0.6$

All samples were found to be n-type conductors at room temperature, which is usual for the manganites with high alkaline-earth content [26,27]. Temperature dependences of the conductivities for the studied compositions in the coordinates $\log(\sigma \cdot T) - 1/T$ are shown in Fig. 12. All the dependences have similar behavior and demonstrate the increase of the σ value from ~1 to ~50 S/cm as the temperature increases from 300 to 1173 K. At temperatures higher than 800 K the conductivity does not depend on the calcium content x, while at lower temperatures the σ values decrease with increasing the calcium content.

The conductivity versus temperature in the range of 300–700 K is in good agreement with a model of a small polaron charge transport, which is known to be a most adequate model for the explanation of the transport properties of distorted manganites and cobaltites with the perovskite-like structure [28–31], see Fig. 12:

$$\sigma \sim \frac{1}{T}\exp\left(-\frac{E_a}{kT} \div\right) \qquad (1)$$

In this formula T is the absolute temperature, k is the Boltzmann coefficient and E_a is the activation energy that
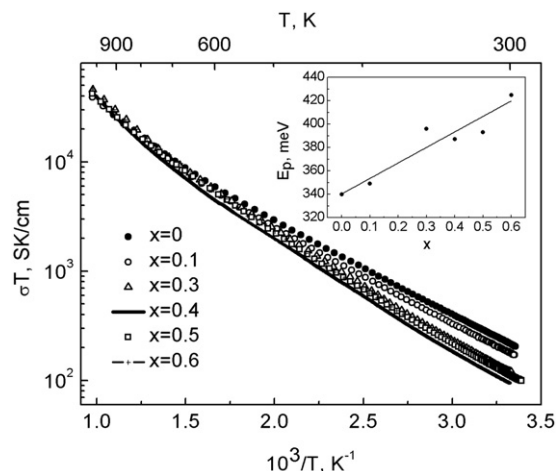
approximately equals to the half of the polaron binding energy E_p ($E_aH \approx E_p/2$).

From the inset in Fig. 12 one can see that the E_p value increases from 340 to 430 meV with an increase of the calcium content from $x=0$ to $x=0.6$. This result could not be interpreted in terms of a cationic disorder [32,33]. This concept states that introducing an additional cation raises the cationic disorder, the local potential fluctuation, and the charge localization, altogether leading to the increase of the polaron binding energy. However, the cation disorder seems to be the same for all studied compositions. Therefore the increase of E_p with the Ca-content is most likely due to narrowing of the valence bandwidth because of the decreasing of the B–O–B angles caused by the increased rotation of the BO_6 octahedra.

4. Discussion

In the present work we have studied the influence of cobalt by manganese substitution in 314-phase ($Sr_{0.75}Y_{0.25}CoO_{2.625}$) and strontium by calcium replacement in the prepared compounds on the crystal structure and high-temperature properties. As in the case of the Fe-substituted 314-phase, the substitution of cobalt by manganese in $Sr_{0.75}Y_{0.25}CoO_{2.625}$ leads to an increase

of the oxygen content if the synthesis is performed in air. This can be explained by a higher stability of the oxidation state $+4$ for manganese in comparison with cobalt. In the Fe-substituted $Sr_{0.75}Y_{0.25}Co_{1-x}Fe_xO_{2.625+y}$ phases, the composition with the 50% substitution of Co by Fe ($x=0.5$) still crystallizes in the ordered structure of the 314-phase [34]. However, in $Sr_{0.75}Y_{0.25}Co_{0.5}Mn_{0.5}O_{2.73}$ we observed the formation of a cubic perovskite phase. In this case the presence of additional oxygen atoms in comparison with $Sr_{0.75}Y_{0.25}Co_{0.5}Fe_{0.5}O_{2.673}$ results in disordering of oxygen vacancies and A-cations in the 314-structure. The average formal oxidation state for B-cations in $Sr_{0.75}Y_{0.25}Co_{0.5}Mn_{0.5}O_{2.73}$ is $+3.2$. Therefore, taking into account that the oxidation state for Co in oxides rarely exceeds $+3$, one can speculate that 40% of manganese cations are present in the form of Mn^{4+}.

Much lower TEC values are observed for the Mn-containing compounds than for the undoped and Fe-substituted 314-phase. For example, for $Sr_{0.75}Y_{0.25}CoO_{2.625}$ $Sr_{0.75}Y_{0.25}Co_{0.5}Fe_{0.5}O_{2.69}$ and $Sr_{0.75}Y_{0.25}Co_{0.25}Fe_{0.75}O_{3-y}$ the TEC values are 19.0, 18.0 and 18.9 ppm K^{-1} (473–1073 K), respectively [18]. They have to be compared with 15.5 and 15.1 ppm K^{-1} for $Sr_{0.75}Y_{0.25}Co_{1-x}Mn_xO_{3-y}$, $x=0.5$ and 0.75, respectively. In all these cases the high TEC values can be attributed to a substantial impact of chemical expansion appearing at $T > 673$ K due to the change of the oxygen stoichiometry. However, the effect of the chemical expansion on TEC in the Mn-substituted compounds is lower in comparison with the undoped and Fe-doped 314-phase. This feature is correlated with the variation of the energy of metal-oxygen bonds in the sequence Mn–Fe–Co, which can be indirectly estimated from the thermodynamic data for different perovskites containing d-elements. Manganese oxides are known to demonstrate higher thermodynamic stability in comparison with iron and cobalt ones in the same oxidation state. For example, the enthalpy (kJ/mol) of the formation of $LaMO_3$ from the elements decreases in a sequence $LaMnO_3$ (-1418.5), $LaFeO_3$ (-1373.5), $LaCoO_3$ (-1241.3) [35,36].

The high-temperature electrical conductivity of $Sr_{0.75}Y_{0.25}Co_{1-x}Mn_xO_{3-y}$ is higher than for the Fe-doped compounds with the corresponding x; e.g., at 1173 K for $x=0.5$, $\sigma=110$ S/cm for M=Mn and $\sigma=63.7$ S/cm for M=Fe [18]. The difference is smaller for $x=0.75$: 44 S/cm and 37.6 for M=Mn and M=Fe, respectively [18]. The temperature dependence of the conductivity is different for the $x=0.5$ and 0.75 samples for both Fe- and Mn-doped compounds. Similar to what reported for the undoped 314-phase, Mn- and Fe-containing perovskites $Sr_{0.75}Y_{0.25}Co_{1-x}M_xO_{3-y}$, $x=0.5$, show the abrupt increase of the conductivity with increasing temperature from room temperature to 1173 K. For example, at 450 K the conductivity of $Sr_{0.75}Y_{0.25}Co_{0.5}Mn_{0.5}O_{3-y}$ is 2 S/cm, which increases up to 110 S/cm at 1173 K, while for $Sr_{0.75}Y_{0.25}Co_{0.25}Mn_{0.75}O_{3-y}$ it is 18 S/cm at 450 K and 44 S/cm at 1173 K. This indicates a different nature of the high-temperature conductivity in these perovskites with different cobalt content.

The distortion of the perovskite structure can be an important parameter to tune when optimizing the TEC of perovskites. It is therefore important to know how the symmetry of the perovskite structure (i.e., degree of octahedra tilting in their structures) influences the thermal expansion behavior. Some information can be found from the high-temperature behavior of perovskites exhibiting temperature induced phase transitions. Ross and Hazen indicate that high-temperature modifications with high symmetry, e.g., cubic perovskites, show higher TEC than low-temperature ones [37]. Later Y. Zhao and Weidner argued that this can only be the case for ferroelectric perovskites [38]. However, in the literature there are examples of perovskites with the centrosymmetric orthorhombic $GdFeO_3$-type structure exhibiting both types of behavior. For example, $NaMgF_3$ undergoes a

phase transition from the $GdFeO_3$-type to a cubic perovskite at 765 °C with a change in volumetric thermal expansion (TEC_v) from 88 to 94.9 ppm K^{-1} [39]. Another example is the increase of TEC for $SrZrO_3$ when it transforms from the low temperature orthorhombic $GdFeO_3$ modification ($TEC_v=29.8$ ppm K^{-1}) to the high-temperature tetragonal one (I 4/ mcm) ($TEC_v=37.5$ ppm K^{-1}) [38]. However, a recent study of the high-temperature crystal structure of $SrZrO_3$ revealed that its high-temperature cubic modification in fact exhibits a lower TEC_v (29 ppm K^{-1}) than the orthorhombic modification ($TEC_v=31.0$ ppm K^{-1}) [40]. Therefore the changes in the TEC behavior on going through the phase transitions apparently deserve more attention.

TEC for $Sr_{0.75-x}Ca_xY_{0.25}Co_{0.25}Mn_{0.75}O_{3-y}$ only slightly decreases with calcium content or with distortion of the perovskite structure (Table 2). However, it is higher or comparable (for $x=0.6$) with the TEC for the undoped $Sr_{0.75}Y_{0.25}Co_{0.25}Mn_{0.75}O_{3-y}$. This indicates that the influence of other factors, like different strength of Ca–O and Sr–O bonds and the variation of the oxygen content with calcium content, should also be taken into account.

High-temperature conductivity properties of $Sr_{0.75-x}Ca_xY_{0.25}Co_{0.25}Mn_{0.75}O_{3-y}$ show a clear dependence on the calcium content. A decrease in the conductivity, especially at low temperatures, and an increase of the activation energy with increasing the calcium content are observed (Fig. 12). This can be explained by the increasing amount of smaller Ca^{2+}, which leads to an increased rotation of the BO_6 octahedra and narrowing of the valence bandwidth due to a decreasing of the B–O–B angles from 180°.

The orthorhombic oxygen-deficient perovskite $Ca_{0.75}Y_{0.25}Mn_{0.85}Co_{0.15}O_{3-y}$ shows substantially lower TEC (13.8 ppm K^1) compared to both $Sr_{0.75}Y_{0.25}Co_{1-x}Mn_xO_{3-y}$, $x=0.5$ and 0.75, and $Sr_{0.75-x}Ca_xY_{0.25}Co_{0.25}Mn_{0.75}O_{3-y}$, $0.1 \leq x \leq 0.6$. Moreover, it exhibits high conductivity of 135 S/cm at 1173 K [20] and can be considered as a good cathode material for SOFC. The reason for the low TEC for $Ca_{0.75}Y_{0.25}Mn_{0.85}Co_{0.15}O_{3-y}$ can be simply explained by a smaller cobalt content, which reduces an influence of the Co^{3+} spin transitions on TEC. The conductivity properties of $Ca_{0.75}Y_{0.25}Mn_{0.85}Co_{0.15}O_{3-y}$ seem to be better described in connection with rare-earth doped $CaMnO_3$. $Ca_{1-x}R_xMnO_3$ compounds are known to exhibit high conductivity and even a metal–insulator (MI) transition at a low doping level [41].

5. Conclusions

The substitution of cobalt in the 314-phase $Sr_{0.75}Y_{0.25}CoO_{2.62}$ by manganese leads to the formation of oxygen deficient compounds $Sr_{0.75}Y_{0.25}Co_{1-x}Mn_xO_{3-y}$, $x=0.5$ and 0.75, with the cubic and orthorhombic perovskite structures. They have an advantage over the undoped compound in lower TEC values, however, their electrical conductivities at high temperatures are lower. In comparison with the Fe-doped 314-phase $Sr_{0.75}Y_{0.25}Co_{1-x}Fe_xO_{2.625+y}$ [18], the Mn-substituted compounds $Sr_{0.75}Y_{0.25}Co_{1-x}Mn_xO_{3-y}$, $x=0.5$, 0.75 demonstrate higher conductivity and lower TEC values. The conductivity of the $x=0.5$ sample (110 S/cm) at 1173 K is substantially higher in comparison with $x=0.75$ (44 S/cm). Together with comparable TEC values for $x=0.5$ (15.5 ppm K^{-1}) and 0.75 (15.1 ppm K^{-1}) samples this makes the former one a promising cathode material for IT-SOFC. Partial replacement of Sr by Ca in $Sr_{0.75}Y_{0.25}Co_{0.25}Mn_{0.75}O_{3-y}$ leads to the formation of the solid solution with the orthorhombic perovskite structure, $Sr_{0.75-x}Ca_xY_{0.25}Co_{0.25}Mn_{0.75}O_{3-y}$, $0.1 \leq y \leq 0.6$. The high-temperature electrical conductivity of $Sr_{0.75-x}Ca_xY_{0.25}Co_{0.25}Mn_{0.75}O_{3-y}$ for entire compositional range is comparable with that for $Sr_{0.75}Y_{0.25}Co_{0.25}Mn_{0.75}O_{3-y}$ and TEC values vary only slightly with calcium content showing no advantage of these materials over $Sr_{0.75}Y_{0.25}Co_{0.25}Mn_{0.75}O_{3-y}$. Along with $Sr_{0.75}Y_{0.25}Co_{0.5}Mn_{0.5}O_{3-y}$, perovskite $Ca_{0.75}$

$Y_{0.25}Mn_{0.85}Co_{0.15}O_{3-y}$ represent promising cathode material for IT-SOFC due to low TEC value (13.8 ppm K^{-1}) and high conductivity of 135 S/cm at 1173 K [20].

Acknowledgments

References

[1] H. Yokokawa, T. Horita, Chapter 5. Cathode, in: S.C. Singhal, K. Kendall (Eds.), High Temperature Solid Oxide Fuel Cells Fundamentals, Design and Application, Elsevier, 2003, pp. 119–147.
[2] H. Yokokawa, Chapter 2. Overview of intermediate-temperature solid oxide fuel cells, in: T. Ishihara (Ed.), Perovskite Oxide For Solid Oxide Fuel Cells, Springer, 2009, pp. 17–43.
[3] S. Uhlenbruck, F. Tietz, Mater. Sci. Eng. B107 (2004) 277–282.
[4] R.D. Shannon, Acta Crystallogr. A32 (1976) 751–767.
[5] F.M. Figueiredo, J.R. Frade, F.M.B. Marques, Solid State Ionics 118 (1999) 81–87.
[6] A. Hammouche, E. Siebert, A. Hammou, Mat. Res. Bull. 24 (1989) 367–380.
[7] R. Chiba, F. Yoshimura, Y. Sakurai, Solid State Ionics 124 (1999) 281–288.
[8] M.B. Phillipps, N.M. Sammes, O. Yamamoto, Solid State Ionics 123 (1999) 131–138.
[9] V.V. Kharton, A.P. Viskup, D.M. Bochkov, E.N. Naumovich, O.P. Reut, Solid State Ionics 110 (1998) 61–68.
[10] L. Qiu, T. Ichikawa, A. Hirano, N. Imanishi, Y. Takeda, Solid State Ionics 158 (2003) 55–65.
[11] H. Lv, Y.-J. Wu, B. Huang, B.-Y. Zhao, K.-A. Hu, Solid State Ionics 177 (2006) 901–906.
[12] C.R. Dyck, R.C. Peterson, Z.B. Yu, V.D. Krstic, Solid State Ionics 176 (2005) 103–108.
[13] H. Lv, B.-Y. Zhao, Y.-J. Wu, G. Sun, G. Chen, K.-A. Hu, Mater. Res. Bull. 42 (2007) 1999–2012.
[14] S.Ya. Istomin, J. Grins, G. Svensson, O.A. Drozhzhin, V.L. Kozhevnikov, E.V. Antipov, J.P. Attfield, Chem. Mater. 15 (2003) 4012–4020.
[15] S.Ya. Istomin, O.A. Drozhzhin, G. Svensson, E.V. Antipov, Solid State Sci. 6 (2004) 539–546.
[16] Y. Li, Y.N. Kim, J. Cheng, J.A. Alonso, Zhiwei Hu, Yi-Ying Chin, T. Takami, M.T. Fernández-Díaz, Hong-Ji Lin, Chien-Te Chen, L.H. Tjeng, A. Manthiram, J.B. Goodenough, Chem. Mater. 23 (2011) 5037–5044.
[17] T. Liu, Y. Li, J.B. Goodenough, J. Power Sources 199 (2012) 161–164.
[18] S.Ya. Istomin, O.A. Drozhzhin, Ph.S. Napolsky, S.N. Putilin, A.A. Gippius, E.V. Antipov, Solid State Ionics 179 (2008) 1054–1057.
[19] I. Burmistrov, O.A. Drozhzhin, S. Ya., V.V. Istomin, E.V. Sinitsyn, Antipov, S.I. Bredikhin, J. Electrochem. Soc. 156 (2009) B1212–B1217.
[20] I.S. Bredikhin, F.S. Napol'skii, E.V. Korovkin, S. Ya., E.V. Istomin, Antipov, S.I. Bredikhin, Russ. J. Electrochem. 45 (2009) 434–438.
[21] R.H. Mitchell, Perovskites: Modern and Ancient, Almaz Press, 2002.
[22] S.Ya. Istomin, V.A. Koutcenko, E.V. Antipov, G. Svensson, J.P. Attfield, J. Mater. Chem. 12 (2002) 2352–2355.
[23] A.C. Larson and R.B. Von Dreele, General Structure Analysis System (GSAS), Los Alamos National Laboratory Report LA-UR-86-748 (2000); B.H. Toby, "EXPGUI, a graphical user interface for GSAS", J. Appl. Cryst. 34 (2001) 210.
[24] C.J. Howard, H.T. Stokes, Acta Crystallogr. B54 (1998) 782–789.
[25] Q. Zhou, B.J. Kennedy, J. Phys. Chem. Solids 67 (2006) 1595–1598.
[26] G.M. Gao, C.L. Chen, Y.C. Wang, Z.M. Song, Phys. B 399 (2007) 17–20.
[27] T. Maitra, A. Taraphder, Phys. Rev. B 68 (2003) 174416.
[28] Y. Lyanda-Geller, S.H. Chun, M.B. Salamon, P.M. Goldbart, P.D. Han, Y. Tomioka, A. Asamitsu, Y. Tokura, Phys. Rev. B. 63 (2001) 184426.
[29] M. Salamon, M. Jaime, Rev. Mod. Phys. 73 (2001) 583–628.
[30] S.R. Sehlin, H.U. Anderson, D.M. Sparlin, Phys. Rev. B 52 (1995) 11681.
[31] D. Emin, Phys. Rev. Lett. 25 (1970) 1751–1755.
[32] H.L. Cai, X.S. Wu, F.Z. Wang, A. Hua, S.S. Jiang, J. Gao, W.S. Tan, J. Alloys Compd. 397 (2005) 250–254.
[33] H. Jain, A.K. Raychaudhuri, Ya.M. Mukovskii, D. Shulyatev, Solid State Commun. 138 (2006) 318–323.
[34] F. Lindberg, O.A. Drozhzhin, S.Ya. Istomin, G. Svensson, F.B. Kaynak, P. Svedlindh, P. Warnicke, A. Wannberg, A. Mellergård, E.V. Antipov, J. Solid State Chem. 179 (2006) 1433–1443.
[35] R.V. Wandekar, B.N. Wani, D. Das, S.R. Bharadwaj, Thermochimica. Acta 493 (2009) 14–18.
[36] J. Cheng, A. Navrotsky, X.-D. Zhou, H.U. Anderson, J. Mater. Res. 20 (2005) 191–200.
[37] N. Ross, R.M. Hazen, Phys Chem. Miner. 6 (1989) 415–420.
[38] Y. Zhao, D. Weidner, Phys. Chem. Miner. 18 (1991) 294–301.
[39] Y. Zhao, D.J. Weidner, J.B. Parise, David E. Cox, Phys. Earth Planet. Inter. 76 (1-16) (1993) 17–34.
[40] S. Hasegawa, T. Sugimoto, T. Hashimoto, Solid State Ionics 181 (2010) 1091–1097.
[41] Y. Wang, Y. Sui, J. Cheng, X. Wang, Z. Lu, W. Su, J. Phys. Chem. C 113 (2009) 12509–12516.